Micro- and nano-bone analyses of the human mandible coronoid process and tendon-bone entheses

Masaaki Kasahara,[1,6] Satoru Matsunaga,[2,6] Tomoko Someya,[1] Kei Kitamura,[3,6] Kento Odaka,[4,6] Takuya Ishimoto,[5] Takayoshi Nakano,[5] Shinichi Abe,[2] Masayuki Hattori[1]

1 Department of Dental Materials Science, Tokyo Dental College, Tokyo, Japan

2 Department of Anatomy, Tokyo Dental College, Tokyo, Japan

3 Department of Histology and Developmental Biology, Tokyo, Japan

4 Department of Oral and Maxillofacial Radiology, Tokyo Dental College, Tokyo, Japan

5 Division of Materials and Manufacturing Science, Graduate School of Engineering, Osaka University, Osaka, Japan

6 Oral Health Science Center, Tokyo Dental College, Tokyo, Japan

Corresponding author: Masaaki Kasahara

Tokyo Dental College, 2-9-18, Misaki-cho, Kanda, Chiyoda-ku, Tokyo 101-0061, Japan

Tel: +81-3-6380-9266

E-mail: kasaharamasaaki@tdc.ac.jp

Abstract

The coronoid process provides attachment to temporalis and masseter muscles, and thus plays an important role in mastication. Tendons connect muscles and bones, mediating the transmission of functional loads to bones. Thus, tendon–bone entheses govern mechanical stress in bones. The preferential orientation of biological apatite (BAp) crystallites, the main mineral component in bones, is an important index for bone quality and function, and is largely influenced by locally applied stress. In this study, we analyzed BAp orientation, Young's modulus, and bone mineral density (BMD) at different sites in the human coronoid process. No differences in BMD were found among the analyzed sites, but BAp crystal orientation was observed to differ. BAp crystallites showed a uni‐directional orientation in the mesiodistal direction at the coronoid process apex, but were oriented in the direction vertical to the occlusal plane at other sites. Young's modulus tended to vary according to the BAp orientation. At the apex, a tendon form with characteristics different from those at other sites, including the presence of a fibrocartilaginous layer that may act as a stretching brake to control stress concentration, was observed. These findings suggest that the functional pressure of the temporalis muscle affects bone quality and strength.

1INTRODUCTION

Tendon entheses into bone join the tendon, which is soft tissue, and bone, which is hard tissue, and are therefore a specific tissue that connects materials with different mechanical properties. Tendon entheses are generally classified into fibrocartilaginous entheses, in which there is a fibrocartilaginous layer between the tendon and bone, and fibrous entheses, in which there is no fibrocartilaginous layer (Apostolakos et al., 2014; Benjamin & Ralphs, 1998; Benjamin & Ralphs, 2002; Doschak & Zernicke, 2005; Lu & Thomopoulos, 2013). It is known that, in the trunk and extremities of humans, fibrocartilaginous entheses are seen in the epiphyseal region of the long bones, the rotator cuff, and the Achilles tendon, while fibrous entheses are seen in the deltoid muscle that terminates in the humerus, the adductor muscle of the femur, and at other sites where muscles attach to long bones in the trunk (Apostolakos et al., 2014). From the standpoint of mechanical properties, sites at which muscles attach via fibrocartilaginous entheses have a larger angle of tendon insertion than sites in which the attachment is a fibrous enthesis, and the fibrocartilaginous layer acts as a shock absorber that prevents inflammation caused by the large movability and chronic use of the joint (Benjamin & Ralphs, 1998; Benjamin & Ralphs, 2002). Conversely, it has been reported that, among tendon entheses of the masticatory muscles, there are some sites at which the tendon inserts directly into the bone without passing through the periosteum (Hems & Tillmann, 2000). Thus, masticatory muscle tendon entheses are of three types: fibrous entheses inserting into the periosteum; fibrous entheses inserting directly into the bone; and fibrocartilaginous entheses. Furthermore, Bittar, Bibb, and Pullinger (1994) reported that, at the pterygoid fovea, which is the terminating point of the lateral pterygoid muscle, both fibrous entheses and fibrocartilaginous entheses are present, and there are still many

aspects pertaining to the relationship between the specific structural properties of tendon entheses in the mandible and the mechanical functions of muscles that are unclear.

In recent years, when bone assessment is done, bone quality, which expresses the structural and material elements of the bone, has been an increasing focus of attention (NIH, 2001), and there are expectations that this can be used as an indicator clarifying the relationship between bone strength and structural properties. In particular, the orientation of biological apatite (BAp) crystallites/collagen, which is an indicator of bone quality, displays a marked reaction to local stress, and it has been reported that evaluating the orientation makes it possible to infer regions that are subject to mechanical stress, and their magnitude and directionality (Ishimoto, Nakano, Umakoshi, Yamamoto, & Tabata, 2013; Morioka et al., 2012; Nakano et al., 2002; Ozasa et al., 2018; Sasaki, Matsushima, Ikawa, Yamamura, & Fukuda, 1989; Sasaki & Sudoh, 1997; Wang, Ishimoto, & Nakano, 2017). Nakano et al. used a microbeam X‐ray diffraction system to conduct quantitative evaluation of the orientation of BAp crystallites in bones in the trunk and extremities of laboratory animals and identified a strong correlation between the mechanical load on bone and BAp crystallite alignment (Nakano et al., 2002). In the human jawbone as well, it has been observed that the orientation of BAp crystallites demonstrates a specific preferred orientation in areas adjacent to teeth, and it has been suggested that occlusal pressure exerts an impact on the structure of bone and on bone strength (Furukawa et al., 2019; Furuya et al., 2012; Kasahara et al., 2016; Miyabe et al., 2007). Because of this, by conducting qualitative analysis of bone at the tendon entheses of masticatory muscles, it should be possible to predict how not only occlusal pressure, but also the functional force of muscles affects the local structure of the mandible with a high degree of accuracy.

Given that, in the present study, histological investigations and analyses of the material mechanics in tendon entheses of the human mandible coronoid process, as well as evaluation of bone mass and bone quality, were carried out with the aim of clarifying some aspects of the micro/nano structural properties of the masticatory muscles, tendons, and bones and the local loading environment.

2 MATERIALS AND METHODS

2.1 Samples

Before conducting the study, dentulous mandibles with temporalis muscles attached were collected from 11 Japanese adult cadavers (average age: 73.17 ± 9.12 years) from the Department of Anatomy, Tokyo Dental College to use as samples. These criteria were set for the selection of cadavers: at least 12 teeth (first and second molar, and one of the premolar teeth, on the left and right of the maxilla and mandible) and no obvious morphological abnormalities or other irregularities. Because molars play a major role in mastication (chewing and grinding), the masticatory condition of cadavers with 12 remaining molar teeth was regarded as equivalent to normal in this study, considering the limited availability of cadavers. Approval (No. 777) was obtained from the Ethics Committee of Tokyo Dental College before beginning the study.

2.2 Preparation of samples

The samples were fixed in 10% neutral buffered formalin solution, following which they were dehydrated in 70% ethanol in preparation for use in the study. The region of interest was from the apex of the coronoid process on the right side to the bottommost point of the mandibular notch, that point being the base of the coronoid process. First, a diamond

cutter (FineCUT, Heiwa Technica, Kanagawa, Japan) was used to excise the coronoid process from the bottommost point of the mandibular notch parallel to and perpendicular to the occlusal plane (Figure 1a). Prior to conducting the various evaluations, three axes were set as reference axes: the X‐axis (in the mesiodistal direction); the Y‐axis (in the vertical direction to the occlusal plane); and the Z‐axis (in the buccolingual direction) (Figure 1a). The harvested coronoid processes were fixed in 4% paraformaldehyde buffer solution and decalcified for 4 weeks using 10% EDTA. The decalcified samples were then embedded in paraffin. To confirm tendon insertion of the temporalis muscle and the coronoid process, thin sliced sections with a thickness of 5 μm were prepared parallel to the Y‐axis in the sagittal direction. To carry out morphological observation of the tissue, H‐E staining was done, and to confirm the fibrocartilaginous layer, toluidine blue staining was performed.Samples for bone quality analysis were prepared by embedding the samples in autopolymer resin (SCANDIPLEX, SCANDIA, Hagen, Germany) and then cutting slices using a saw microtome having a blade width of 300 μm (SP1600, Leica, Wetzlar, Germany) and partitioning them into sagittal sections parallel to the Y‐axis. In order to remove the rough surface from the sections, a grinder (ECOMET3, BUEHLER, Uzwil, Switzerland) was used to grind the slices using waterproof abrasive paper (#400 → #800 → #1200). For the final finishing, colloidal silica with a particle size of 0.05 μm was used to polish the surfaces. The samples for X‐ray diffraction were prepared to a thickness of 200 μm, while those for nanoindentation were prepared to a thickness of 2 mm.

2.3 Setting of measurement sites

Seven sites (a through g) around the perimeter of the coronoid process cortical bone were

set (Figure 1b) as the sites for measurements of bone mineral density (BMD), the X‐ray diffraction analysis intensity ratio, and Young's modulus. The cortical bone directly under the tendon enthesis of the coronoid process apex was set as point A. Next, a straight line was drawn from point A to the central part of the base of the coronoid process. Vertical lines were then drawn that divided the straight line into three equal parts, with points B, C, and D being set for the cortical bone at the base of the mesial coronoid process, and points E, F, and G being set for the center part of the distal coronoid process base cortical bone.

2.4 Scanning electron microscopy

To observe the cortical bone structure of the sample cross‐sections, a scanning electron microscope (SU6600, Hitachi, Japan) was used. As for measurement points, the Haversian canal was avoided, and the interstitial lamellae surrounding osteons were selected (Nakano et al., 2002).

2.5 Measurement of bone mineral density

The harvested samples were photographed using micro‐computed tomography (μCT) (HMX225Actis4, Tesco Corporation, Japan) at 140 kV and 93 μA with a spatial resolution of $50 \times 50 \times 50\ \mu m^3$. For quantitative analysis of BMD, a set of BMD phantoms with X‐ray absorption coefficients equivalent to BMDs of 800, 700, 600, 500, 400, 300, and 200 mg/cm^3 (Ratoc System Engineering Corporation, Tokyo, Japan) were scanned with the same condition. After carrying out three‐dimensional construction based on the images that were obtained, the volume of $0.5 \times 0.5 \times t\ mm^3$ (t depended on the thickness of coronoid process) was extracted. The CT gray‐value of the samples was converted to

BMD using the scan data of the BMD phantoms by a 3D analysis software (TRI/3D‐BON, Ratoc System Engineering Corporation).

2.6 Biological apatite (BAp) crystallite alignment

Quantitative analysis of the BAp crystallite alignment was performed using an X‐ray diffraction system (D/MAX RAPIDII‐CMF, Rigaku Corporation, Tokyo, Japan). Measurements were obtained using two types of optical systems: transmission and reflection optical systems. With both systems, the Cu‐Kα line was used as the source. The tube voltage was set to 40 kV and the tube current to 30 mA. The irradiated site was determined using an optical microscope (magnification: ×4.8). X‐rays were collimated into a circular spot with a diameter of 100 μm. The diffracted X‐ray beam was detected with an optical curved imaging plate. The X‐ray diffraction intensities were collected in the X‐, Y‐, and Z‐axis directions. The measurement conditions were set based on the method used by Miyabe et al. (2007) for the transmission optical system and Nakano et al. (2002) for the reflection optical system. The diffraction intensity in the X‐axis direction was measured using a reflection optical system, whereas measurements in the Y‐ and Z‐axis directions were performed using a transmission optical system. The incident X‐ray was radiated on the sample surface in consideration of Bragg angles of (002) and (310) peaks, $\theta = 12.95°$ and 19.9°, respectively. The data were recorded for 120 s. Using 2D data processing software (Rigaku Corporation, Tokyo, Japan), the X‐ray intensity ratios of the two diffraction peaks of the (002) and (310) planes were calculated. This has previously been reported as a suitable index for evaluating apatite orientation (Nakano, Kaibara, Ishimoto, Tabata, & Umakoshi, 2012 Nakano et al., 2002). Three measurements were obtained for each point, and the data were averaged. The X‐

ray diffraction intensity ratio of nonoriented apatite powder was 1.84 for the transmission type and 1.06 for the reflection type.

2.7 Determination of Young's modulus

The Young's modulus for the various measurement points was calculated using a load control type of nanoindentation system (ENT‐1100a, ELIONIX Corporation, Tokyo, Japan). Three orthogonal surfaces perpendicular to X‐, Y‐, and Z‐axis directions were prepared at each point (A–G) in order to measure the Young's modulus in the three directions. The samples were placed in a shielding case in which the temperature could be adjusted to 28.0 ± 0.1°C and left for 1 day, after which measurements were carried out. A diamond Berkovich pyramidal indenter was used for all measurements. Using a CCD camera and optical microscope connected to the nanoindentation system, the interstitial lamellae to be targeted were selected. Young's modulus was measured using the nanoindentation system according to the method described previously (Ishimoto, Nakano, Yamamoto, & Tabata, 2011). Measurements were done with the loading/unloading rate and maximum load set to 400 μN/s and 6 mN, respectively. To minimize the effects of viscoelastic deformation of the bone during unloading, the load retention time at the time of maximum load was set to 180 s (Ishimoto et al., 2011). Measurement was carried out three times, and the mean values were calculated.

2.8 Statistical analysis

Quantitative results are expressed as mean ± standard deviation (SD) and as individual data plots. The statistical significance of differences among the means was determined

using one‐way repeated measures analysis of variance (ANOVA) or one‐way ANOVA with post hoc multiple comparison analyses. For multiple comparison analyses, Tukey honestly significant difference comparisons were conducted after determining the homoscedasticity of data. p values less than .05 were considered significant. SPSS Statistics version 25 (SPSS Japan Inc., Tokyo, Japan) for Microsoft Windows was used for statistical analyses.

3 RESULTS

3.1 Observation of the cortical bone surface

A scanning electron microscope was used to observe the cross‐section of the cortical bone with a magnification of ×110 (Figure 2). In the cortical bone, normal osteons and the surrounding interstitial lamellae were observed. It was confirmed that the interstitial lamellae could be sufficiently targeted using an incident beam with a diameter of 100 μm.

3.2 Histological observation of tendon entheses

Figure 3 shows the H‐E stained images (a, b, e, g) of the sagittal cross‐sections of the coronoid process, as well as the images stained with toluidine blue (c, d, f, h). In the overall images of the coronoid process, it was confirmed that the marrow space was narrow, with a thick cortical bone structure on the exterior. Moreover, the course of the attached tendons was observed to be in the X‐axis and Y‐axis directions (Figure 3a). In the h–e stained images showing magnified images of the mesial surface cortical bone, the course of the tendon was observed to be in the Y‐axis direction (Figure 3e, black arrow). A fibrous membrane was also observed on the surface layer of the cortical bone

(Figure 3e, asterisk). In magnified images of the distal surface of the cortical bone, the course of the tendon was observed in the X‐axis direction, and the tendon was inserted directly into the bone (Figure 3g, black arrow). Conversely, magnified images of the coronoid process apex showed that the tendon ran in both the X‐ and Y‐axis directions (Figure 3b, black arrows).In the images stained with toluidine blue, a thick fibrocartilaginous layer was confirmed in the cortical bone area at the apex of the coronoid process (Figure 3c). Additionally, magnified images of the fibrocartilaginous layer showed cartilage cells in the interior (Figure 3d, white arrows). No fibrocartilaginous layer was observed in the mesial cortical bone or the distal cortical bone (Figure 3f,h).

3.3 Bone mineral density

Figure 4 shows the results of the BMD quantitative evaluations at the various measurement points (A–G) of the sagittal cross‐section. No significant differences among the measurement points were observed.

3.4 BAp alignment

Figure 5 shows the X‐ray diffraction intensity ratios for the various measurement points. For point A, which is the apex of the coronoid process, a high degree of preferred orientation could be seen in the X‐axis direction, but at points B through G, which are mesial and distal cortical bone, a preferred orientation could be seen in the Y‐axis direction. Conversely, the X‐ray diffraction intensity ratios in the Z‐axis direction were uniformly low values for all of the regions.

3.5 Young's modulus

Figure 6 shows the measurement results for Young's modulus in the X‐, Y‐, and Z‐axis directions. For point A, a high Young's modulus was demonstrated in the X‐axis direction. At all of the measurement points, the Young's modulus of the Y‐axis direction was higher than for the other axis directions.

4 DISCUSSION

Because tendons transfer load from muscles to bones, stress tends to be concentrated at tendon entheses, and these sites are highly vulnerable to injury. To alleviate this concentration of stress and enable efficient load transfer, the tissue layers making up the tendon entheses in the trunk and extremities are significantly different in terms of composition, construction, and mechanical properties, and they exhibit complicated hierarchical structures (Apostolakos et al., 2014). Based on the histological observation of tendon entheses carried out in the present study, a fibrocartilaginous layer was identified only at the apex of the coronoid process. This is consistent with reports by Hems and Tillmann (2000). At the same time, however, Hem et al. reported that the sites at which other tendons attach to the coronoid process exhibit fibrous entheses that attach directly to bone. In the present study, tendons that were inserted through a thick fibrous membrane were observed in mesial cortical bone areas. Because of differences in the course of tendons, and because it was present in the surface layer of the cortical bone, this fibrous membrane could possibly be a fibrous layer of thick periosteum. However, no fibrocartilaginous layer or periosteum was observed in distal cortical bone, and the tendons inserted directly into the bone. Consequently, among coronoid process entheses, only the enthesis at the apex of the coronoid process was a fibrocartilaginous enthesis,

while in mesial areas, attachment sites were fibrous entheses that passed through the periosteum, and attachment sites in distal areas were entheses that inserted directly into bone, without passing through the periosteum. These findings suggest that this is a specific type of tissue in which three different types of entheses are present. Moreover, it has been reported that chondrocytes act as a kind of "stretching brake" that prevents stress from being concentrated at bone interfaces (Benjamin, Evans, & Copp, 1986; Hems & Tillmann, 2000). This suggests that tendon entheses at the apex of the coronoid process are areas at which stress is seen to concentrate, because the functional pressure of muscles might be transmitted through the tendon. No significant differences in BMD were seen at the various measurement points. Past reports have described comparisons between laboratory animals in which muscle functional pressure was reduced or nullified and control animals, and no significant differences in BMD were seen in any of the animals (Bacon, Bacon, & Griffiths, 1980; Tsai, Huang, Lee, Hsiao, & Yang, 2010). Other reports have found no significant differences in the effects of occlusal pressure on the human jawbone (Furukawa et al., 2019; Furuya et al., 2012; Kasahara et al., 2016; Morioka et al., 2012). Because of this, local evaluation of the effects of various types of functional pressure using BMD alone is thought to be highly problematic. Bacon et al. used neutron beams to measure BAp crystallite orientation over the entire area of the coronoid process in human mandibular bone, and they reported that a preferred orientation was observed in the muscle insertion direction of the temporalis muscle (Picard, Lapointe, Brown, & Guertin, 2008). This is largely consistent with the course of tendons seen in the histological examinations in the present study. However, with the micro‐area X‐ray diffraction method used in the present study, the direction of orientation was confirmed to be significantly different depending on the site, being in the X‐axis direction at the

apex of the coronoid process and in the Y‐axis direction at other sites. This suggests that, for the coronoid process, the direction of attachment of the temporalis muscle varies depending on the local site, and that the BAp crystallites also exhibit a preferred orientation locally in various directions in response to the course of the tendon attaching from the temporalis muscle. Furthermore, in the present study, the Young's modulus for coronoid process cortical bone was high, consistent with the orientation direction of the BAp crystallites. Nakano et al. demonstrated that the Young's modulus and other mechanical functions had a stronger correlation with the BAp crystallite orientation than with BMD (Ishimoto et al., 2013; Ishimoto et al., 2019; Sekita et al., 2016; Shinno et al., 2016). The above results suggest that the coronoid process, in response to the functional pressure applied from the temporalis muscle, locally optimizes the microstructure properties of the tendon‐bone entheses for fibrocartilaginous coupling, and it has high mechanical functions as a result of high bone quality in the tendon attachment direction.

The effect of formalin fixation and dehydration on the Young's modulus of the bone specimen should be considered. Formalin fixation has been reported to have little effect on Young's modulus (Ishimoto et al., 2013; Stefan, Michael, & Werner, 2010). Dehydration, in contrast, increases the absolute values of Young's modulus (Bushby, Ferguson, & Boyde, 2004; Rho & Pharr, 1999). However, the relative magnitudes of the modulus remain consistent even after specimens are dehydrated, as confirmed by Rho and Pharr (1999). Thus, the effects of formalin fixation and dehydration would not change our conclusions. These results suggest that mastication has an effect on bone microstructure and functionality. Investigating the effect of tooth loss on microstructure and functionality of the jawbone would be very important in an aging society, and needs to be the focus of further research.

5 CONCLUSION

In the human coronoid process, BAp crystallites showed a uni‐directional orientation in the mesiodistal direction at the apex in which there is a fibrocartilaginous coupling, but were oriented in the direction vertical to the occlusal plane at other sites. Consequently, it is surmised that the functional pressure of the temporalis muscle through the tendon entheses strongly affects the quality and strength of bones.

ACKNOWLEDGMENTS

This work was supported by Grants‐in‐Aid for Scientific Research (Young Scientists B, grant number JP18K45678), and performed under the inter‐university cooperative research program (proposal no. 19G0014) of the Cooperative Research and Development Center for Advanced Materials, Institute for Materials Research, Tohoku University.

CONFLICT OF INTEREST

The authors declare that there is no conflict of interest.

REFERENCE

Apostolakos, J., Durant, T. J., Dwyer, C. R., Russell, R. P., Weinreb, J. H., Alaee, F., … Mazzocca, A. D. (2014). The enthesis: A review of the tendon‐to‐bone insertion. Muscle, Ligaments and Tendons Journal, 4, 33– 42.

Bacon, G. E., Bacon, P. J., & Griffiths, R. K. (1980). Orientation of apatite crystals in relation to muscle attachment in the mandible. Journal of Biomechanics, 13, 725– 729.

Benjamin, M., Evans, E. J., & Copp, L. (1986). The histology of tendon attachments to bone in man. Journal of Anatomy, 149, 89– 100.

Benjamin, M., & Ralphs, J. R. (1998). Fibrocartilage in tendons and ligaments—An adaptation to compressive load. Journal of Anatomy, 193, 481– 494.

Benjamin, M., & Ralphs, J. R. (2002). The skeletal attachment of tendons—tendon "entheses". Comparative Biochemistry and Physiology. Part A, Molecular & Integrative Physiology, 133, 931– 945.

Bittar, G. T., Bibb, C. A., & Pullinger, A. G. (1994). Histologic characteristics of the lateral pterygoid muscle insertion to the temporomandibular joint. Journal of Orofacial Pain, 8, 243– 249.

Bushby, A. J., Ferguson, V. L., & Boyde, A. (2004). Nanoindentation of bone: Comparison of specimens tested in liquid and embedded in polymethylmethacrylate.

Journal of Materials Research, 19, 249– 259.

Doschak, M. R., & Zernicke, R. F. (2005). Structure, function and adaptation of bone‐tendon and bone‐ligament complexes. Journal of Musculoskeletal & Neuronal Interactions, 5, 35– 40.

Furukawa, T., Matsunaga, S., Morioka, T., Nakano, T., Abe, S., Yoshinari, M., & Yajima, Y. (2019). Study on bone quality in the human mandible‐alignment of biological apatite crystallites. Journal of Biomedical Materials Research. Part B, Applied Biomaterials, 107, 838– 846.

Furuya, H., Matsunaga, S., Tamatsu, Y., Nakano, T., Yoshinari, M., Abe, S., & Ide, Y. (2012). Analysis of biological apatite crystal orientation in anterior cortical bone of human mandible using microbeam X‐ray diffractometry. Materials Transactions, 53, 980– 984.

Hems, T., & Tillmann, B. (2000). Tendon entheses of the human masticatory muscles. Anatomy and Embryology, 202, 201– 208.

Ishimoto, T., Nakano, T., Umakoshi, Y., Yamamoto, M., & Tabata, Y. (2013). Degree of biological apatite c‐axis orientation rather than bone mineral density controls mechanical function in bone regenerated using recombinant bone morphogenetic protein‐2. Journal of Bone and Mineral Research, 28, 1170– 1179.

Ishimoto, T., Nakano, T., Yamamoto, M., & Tabata, Y. (2011). Biomechanical evaluation of regenerating long bone by nanoindentation. Journal of Materials Science. Materials in Medicine, 22, 969– 976.

Ishimoto, T., Suetoshi, R., Cretin, D., Hagihara, K., Hashimoto, J., Kobayashi, A., & Nakano, N. (2019). Quantitative ultrasound (QUS) axial transmission method reflects anisotropy in micro‐arrangement of apatite crystallites in human long bones: A study with 3‐MHz‐frequency ultrasound. Bone, 127, 82– 90.

Kasahara, M., Matsunaga, S., Odaka, K., Ishimoto, T., Nakano, T., Yoshinari, M., & Abe, S. (2016). Biological apatite crystallite alignment analysis of human maxillary molar region cortical bone with microbeam X‐ray diffraction. Journal of Hard Tissue Biology, 25, 109– 114.

Lu, H. H., & Thomopoulos, S. (2013). Functional attachment of soft tissues to bone: Development, healing, and tissue engineering. Annual Review of Biomedical Engineering, 15, 201– 226.

Miyabe, N. T., Ishimoto, T., Takano, N., Adachi, T., Iwaki, H., Kobayashi, A., & Umakoshi, Y. (2007). Two‐dimensional quantitative analysis of preferential alignment of BAp c‐axis for isolated human trabecular bone using microbeam X‐ray diffractometer with a transmission optical system. Materials Transactions, 48, 343– 347.

Morioka, T., Matsunaga, S., Yoshinari, M., Ide, Y., Nakano, T., Sekine, H., & Yajima, Y.

(2012). Alignment of biological apatite crystallites at first molar in human mandible cortical bone. Cranio, 30, 32– 40.

Nakano, T., Kaibara, K., Tabata, Y., Nagata, N., Enomoto, S., Marukawa, E., & Umakoshi, Y. (2002). Unique alignment and texture of biological apatite crystallites in typical calcified tissues analyzed by microbeam X‐ray diffractometer system. Bone, 31, 479–487.

Nakano, T., Kaibara, K., Ishimoto, T., Tabata, Y., & Umakoshi, Y. (2012). Biological apatite (BAp) crystallographic orientation and texture as a new index for assessing the microstructure and function of bone regenerated by tissue engineering. Bone, 51, 741–747.

NIH. 2001. NIH consensus development panel on osteoporosis prevention, diagnosis, and therapy. 285, 785–795.

Ozasa, R., Ishimoto, T., Miyabe, S., Hashimoto, J., Hirao, M., Yoshikawa, H., & Nakano, T. (2018). Osteoporosis changes collagen/apatite orientation and Young's modulus in vertebral cortical bone of rat. Calcified Tissue International, 104, 449– 460.

Picard, S., Lapointe, N., Brown, J., & Guertin, P. (2008). Histomorphometric and densitometric changes in the femora of spinal cord transected mice. The Anatomical Record, 291, 303– 307.

Rho, J. Y., & Pharr, G. M. (1999). Effects of drying on the mechanical properties of bovine femur measured by nanoindentation. Journal of Materials Science. Materials in Medicine, 10, 485– 488.

Sasaki, N., Matsushima, N., Ikawa, T., Yamamura, H., & Fukuda, A. (1989). Orientation of bone mineral and its role in the anisotropic mechanical properties of bone‐transverse anisotropy. Journal of Biomechanics, 22, 157– 164.

Sasaki, N., & Sudoh, Y. (1997). X‐ray pole figure analysis of apatite crystals and collagen molecules in bone. Calcified Tissue International, 60, 361– 367.

Sekita, A., Matsugaki, A., Ishimoto, T., & Nakano, T. (2016). Synchronous disruption of anisotropic arrangement of the osteocyte network and collagen/apatite in melanoma bone metastasis. Journal of Structural Biology, 197, 260– 270.

Shinno, Y., Ishimoto, T., Saito, M., Uemura, R., Arino, M., Marumo, K., … Hayashi, M. (2016). Comprehensive analyses of how tubule occulusion and advanced glycation end‐products diminish strength of aged dentin. Scientific Reports, 6, 19849.

Stefan, U., Michael, B., & Werner, S. (2010). Effects of three different preservation methods on the mechanical properties of human and bovine cortical bone. Bone, 47, 1048– 1053.

Tsai, C., Huang, R., Lee, C., Hsiao, W., & Yang, L. (2010). Morphologic and bony

structural changes in the mandible after a unilateral injection of botulinum neurotoxin in adult rats. Journal of Oral and Maxillofacial Surgery, 68, 1081– 1087.

Wang, J., Ishimoto, T., & Nakano, T. (2017). Unloading‐induced degradation of the anisotropic arrangement of collagen/apatite in rat femurs. Calcified Tissue International, 100, 87– 97.

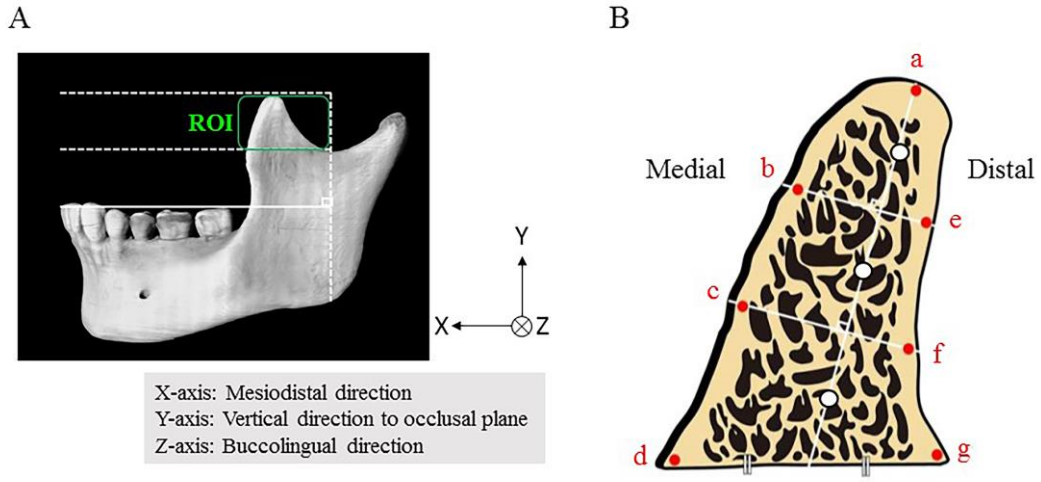

Figure 1

Setting of the region of interest (ROI), coordinate axes, and measurement points for the coronoid process of the human mandible. (a) The ROI was from the apex of the coronoid process on the right side to the bottom‐most point of the mandibular notch, the base of the coronoid process. The coronoid process was excised from the bottom‐most section of the mandibular notch parallel to and perpendicular to the occlusal plane. (b) Seven points (A through G) around the perimeter of the coronoid process cortical bone were selected for analyses. The symbols ‖ and ○ indicate equal line segment lengths

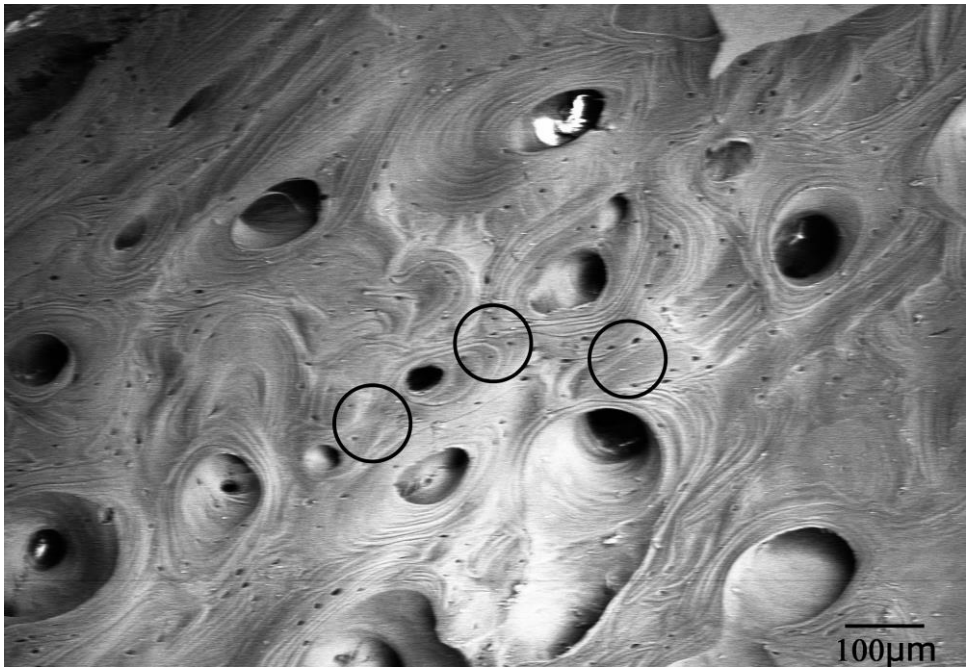

Figure 2

Evaluation using scanning electron microscopy images. The photo shows the coronoid process cortical bone. The circles indicate a collimator beam size of 100 µm. Interstitial lamellae surrounding osteons are confirmed

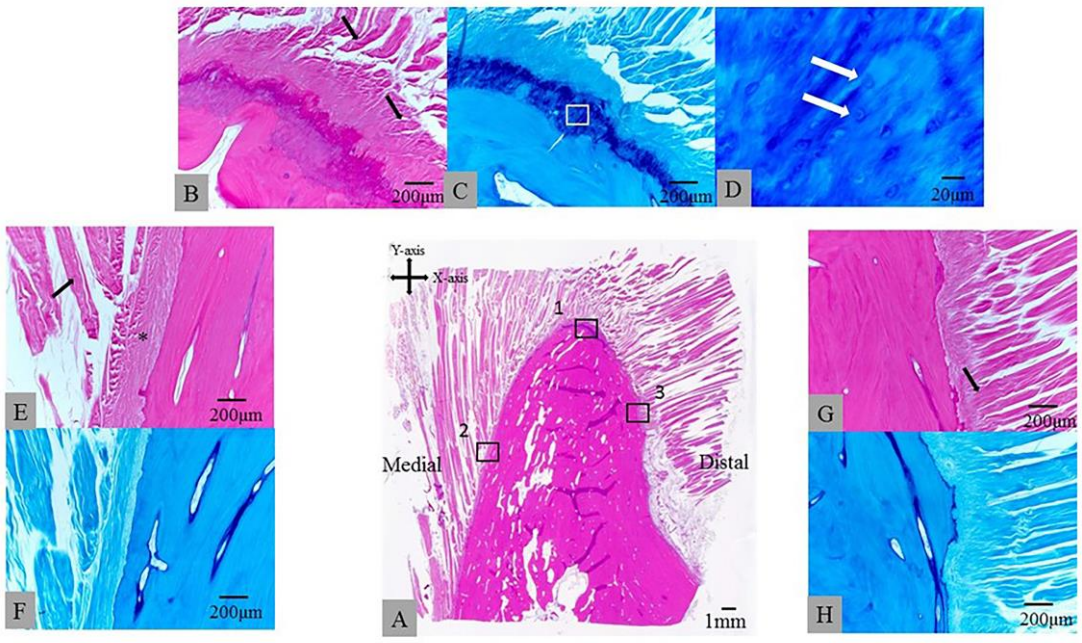

Figure 3

Sagittal‐section coronoid process H‐E stains (a, b, e, g) and toluidine blue stains (c, d, f, h). Panels b–d,e and f, and g and h are magnified images taken in the equivalent squared regions 1–3, respectively. (a) Overall image of sagittal‐section cortical bone (H‐E stained). The marrow space is narrow, with a thick cortical bone structure. Inserted tendons are observed running in the X‐ and Y‐axis. (b) Magnified image of the coronoid process apex (H‐E stained). Tendons running in the Y‐ and X‐axes are observed (black arrows). (c) Magnified image of the coronoid process apex (toluidine blue stained). A thick fibrocartilaginous layer is observed. (d) Magnified image of the squared region in panel c. Fibrocartilaginous cells are seen in the fibrocartilaginous layer (white arrows). (e) Magnified image of the mesial coronoid process (H‐E stained). Tendons running in the Y‐axis (black arrow) and a thick fibrous membrane (asterisk) are observed. (g) Magnified image of the distal coronoid process (H‐E stained). Tendons running in the X‐axis direction are observed (black arrow). (f and h) Magnified images

of the mesial and distal coronoid processes (toluidine blue stained). No fibrocartilaginous layer is observed

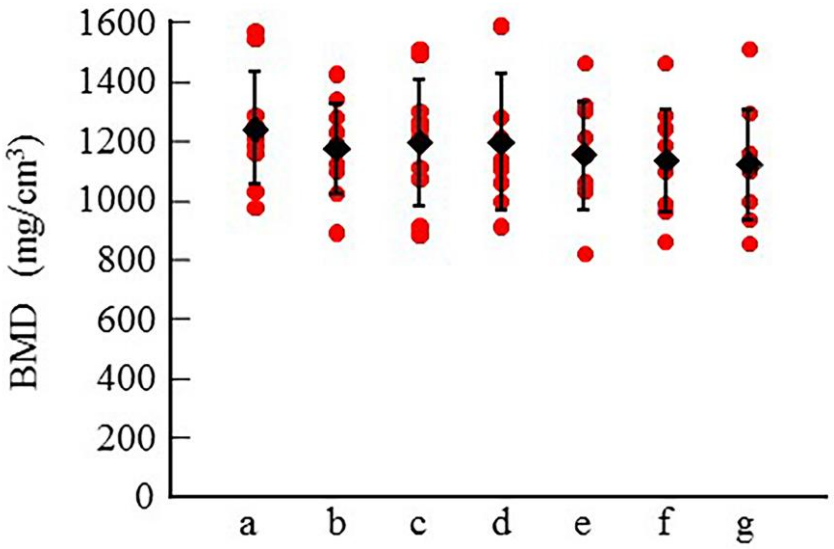

Figure 4

Evaluation of the bone mineral density (BMD) of coronoid process cortical bone. There are no significant differences in the BMD values among the measurement points

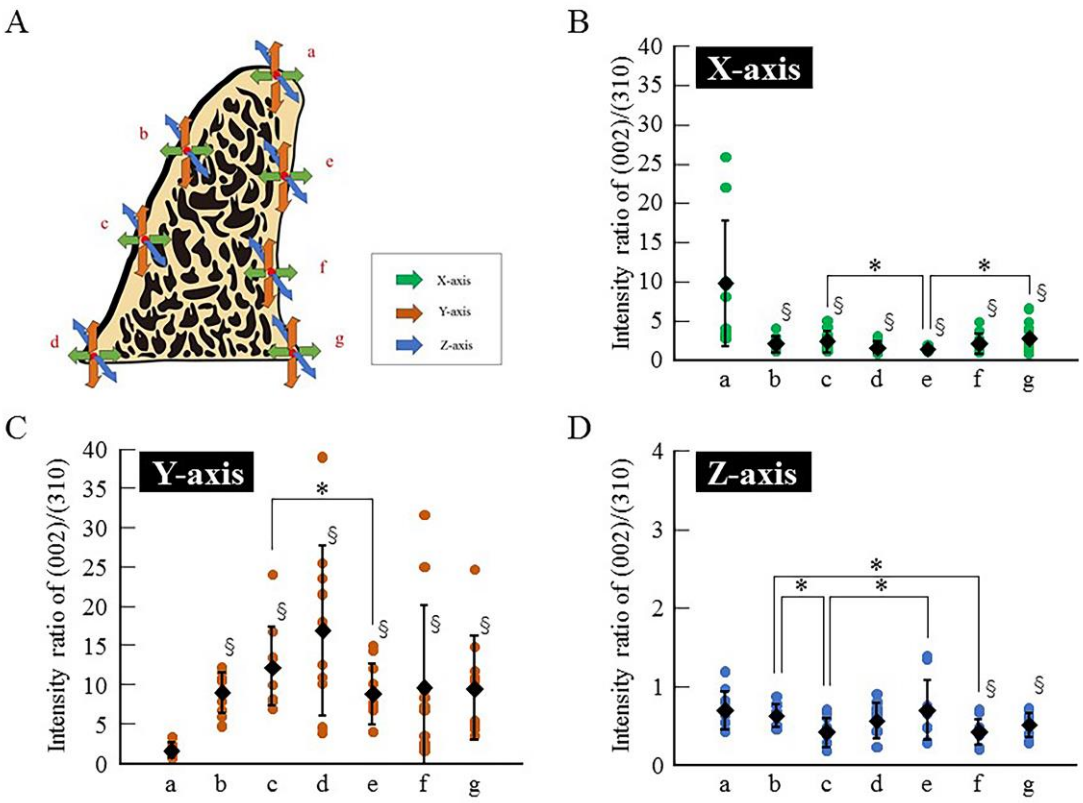

Figure 5

Diffraction intensity ratios along the X‐, Y‐, and Z‐axis representing the preferential BAp c‐axis orientation. (a) Representation of three orthogonal axes in which the BAp orientation analyses were performed. (b–d) Variation in the preferential BAp c‐axis orientation among the analysis points in the X‐, Y‐, and Z‐axis directions. For point A, which is the apex of the coronoid process, a high degree of preferred orientation can be seen in the X‐axis direction. At points B through G, which are located on the mesial and distal cortical bone, a preferred orientation can be seen in the Y‐axis direction. The X‐ray diffraction intensity ratios in the Z‐axis directions are uniformly low for all regions. Note that the scale of the vertical axis is 10‐fold larger in (d). §: $p < .05$ versus point A, *: $p < .05$ between the two means

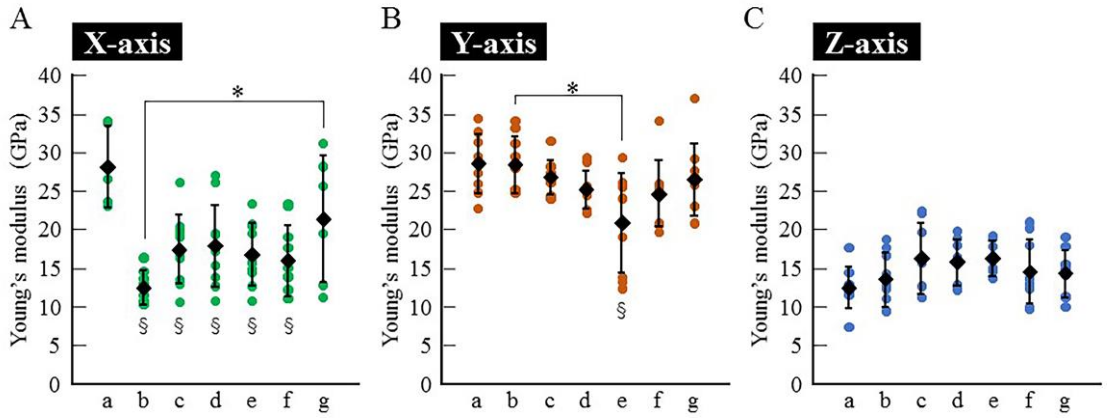

Figure 6

Young's moduli measured in the X‐, Y‐, and Z‐axes. In the X‐axis direction, a high longitudinal elasticity modulus is seen at point A. At all measurement points, the Young's modulus in the Y‐axis direction is higher than that of the other axis directions. §: $p < .05$ versus point A, *: $p < .05$ between the two means